Journal of Sound and Vibration (1979) **65**(2), 275–296

A MAGNETOELASTIC STRANGE ATTRACTOR

F. C. MOON AND P. J. HOLMES

Department of Theoretical and Applied Mechanics, Cornell University, Ithaca, New York 14853, *U.S.A.*

(*Received* 17 *November* 1978, *and in revised form* 5 *April* 1979)

Experimental evidence is presented for chaotic type non-periodic motions of a deterministic magnetoelastic oscillator. These motions are analogous to solutions in non-linear dynamic systems possessing what have been called "strange attractors". In the experiments described below a ferromagnetic beam buckled between two magnets undergoes forced oscillations. Although the applied force is sinusoidal, nevertheless bounded, non-periodic, apparently chaotic motions result due to jumps between two or three stable equilibrium positions. A frequency analysis of the motion shows a broad spectrum of frequencies below the driving frequency. Also the distribution of zero crossing times shows a broad spectrum of times greater than the forcing period. The driving amplitude and frequency parameters required for these non-periodic motions are determined experimentally. A continuum model based on linear elastic and non-linear magnetic forces is developed and it is shown that this can be reduced to a single degree of freedom oscillator which exhibits chaotic solutions very similar to those observed experimentally. Thus, both experimental and theoretical evidence for the existence of a strange attractor in a deterministic dynamical system is presented.

1. INTRODUCTION

Recently a number of papers have appeared in which deterministic, non-linear differential equations exhibiting non-periodic, bounded solutions have been discussed (e.g., references [1–6]). While the equations admit no random parameters or inputs, the resulting oscillations appear to be chaotic and unpredictable. Systems exhibiting such motions have been termed as possessing "strange attractors" in contrast to those having only more regular or predictable motions such as those in regions near equilibrium points and limit cycles. Mathematical models of strange attractors have been postulated for vibrations of a buckled beam [2–4], geomagnetic reversals [5–6], and fluid instabilities [1]. In this paper we present what we believe is the first experimental evidence for the existence of strange attractor motions in structural mechanics. In these experiments magnetic forces are used to buckle a beam and the non-linear oscillations of the buckled beam are examined.

Many technical devices such as motors, generators, transformers, MHD devices, and fusion reactors employ elastic structures in magnetic fields. It has also been shown that flexible structures either of ferromagnetic material or carrying large currents can buckle in magnetic fields [7–9]. Thus the buckled magnetoelastic oscillator might have technical applications in addition to serving as a convenient laboratory model for the study of strange attractor motions.

Strange attractor oscillations have been studied for third order autonomous differential equations, for example in the work of Lorenz [1]. More recently an externally forced non-linear second order oscillator has been shown to exhibit chaotic behavior [2–4]. In this work results from the qualitative theory of dynamical systems and analog computer experiments each played an important part.

The second order strange attractor is characterized by the existence of at least three equilibrium positions in the unforced state: two stable and the other unstable. Such a

0022-460X/79/140275+22 $02.00/0

condition obtains for the post-buckled state of a beam-column under axial load. When a moderate periodic force is applied to the system, the beam jumps from motion about one point to motion about the other in what appears to be a chaotic manner.

If the motion of the beam can be reduced to one mode, then upon using a Galerkin type approximation, a second order differential equation of the following form is obtained, where A and t have been non-dimensionalized:

$$\ddot{A} + \gamma\dot{A} - \tfrac{1}{2}(1 - A^2)A = f\cos\omega t,\ \gamma, f, \omega > 0. \tag{1}$$

When $f = 0$ this system has three equilibria, at $(A, \dot{A}) = (0, 0)$ and $(\pm 1, 0)$. If $\gamma > \varepsilon_0 > 0$ then, for small forces, $f \ll \varepsilon_0$, it can be shown that there are attracting periodic orbits near the latter points and a saddle-type periodic orbit near $(A, \dot{A}) = (0, 0)$ [2]. Linearizing equation (1) about $(A, \dot{A}) = (\pm 1, 0)$ gives a second order system with natural frequency $\omega_0 = 1$. The behavior of equation (1) for increasing values of f is discussed in section 4 and it is shown that extremely complicated sets of periodic and non-periodic orbits appear.

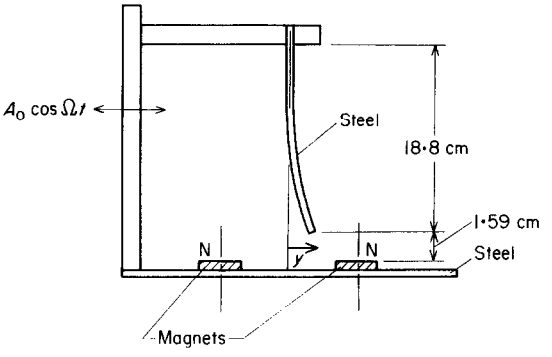

Figure 1. Experimental apparatus, showing ferroelastic beam and permanent magnets.

In the experiments to be described in section 5, magnetic forces were used to buckle a cantilevered ferromagnetic beam. Magnetic forces have the advantage that they do not add mass to the structure and can be changed quite easily. A sketch of the experimental apparatus is shown in Figure 1 and a typical record showing the chaotic motions appears in Figure 2.

In sections 2–4 the magnetic forces on the beam are described and a second order equation of the form (1) is derived. The magnetic forces are shown to lead to either three equilibrium points or five equilibrium points for various positions of the magnets. The bifurcations are

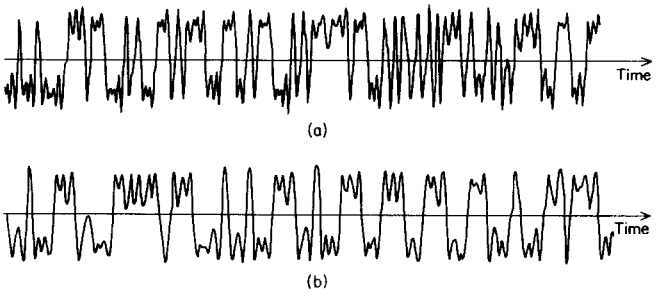

Figure 2. "Strange" attractor vibration records of (a) magnetoelastic beam, $\gamma = 0{\cdot}0036$, $f = 0{\cdot}035$, $\omega = 0{\cdot}89$ and (b) analog computer study of Holmes [2, 3], $\gamma = 0{\cdot}045$, $f = 0{\cdot}28$, $\omega = 0{\cdot}84$.

described by a butterfly catastrophe for the static problem. By analogy with equation (1) the dynamic model is shown to lead to "strange" oscillations about either two or three stable equilibrium points. A more general non-linear partial differential equation is also presented which incorporates non-linear magnetic and linear elastic forces which can be reduced to the single mode model.

Finally, with the mathematical relevance of the magnetoelastic oscillator to the system (1) having been established, experiments are described in section 5 and results presented which exhibit behavior characteristic of strange attractors.

2. THEORETICAL MODELS

2.1. MAGNETIC FORCES

Magnetic forces in solids result from either interaction of electric currents or magnetization with external magnetic fields. In the present problem no electric currents are present and permanent magnets external to the beam create a static, inhomogeneous magnetic field. This field induces a magnetization **M** per unit volume in the solid. The steel beam can be modelled as a soft magnetic material where **M** is proportional to the local magnetic field in the solid; i.e.,

$$\mathbf{M} = [\chi/(\chi + 1)]\,\mathbf{B}/\mu_0, \tag{2}$$

where μ_0 is the magnetic permeability of a vacuum ($4\pi \times 10^{-7}$ MKS units) and χ is the magnetic susceptibility (for steel $\chi \sim 10^3 - 10^4$).

The field **B** can be written in terms of the field $\mathbf{B}^0$ produced by the external magnets, and a field produced by the magnetization itself, $\mathbf{B}^1$. If self-forces on the beam are neglected then the external magnets produce both a force and moment distribution on the beam **F**, **C** (see, e.g., references [7–9]) given by

$$\mathbf{F} = \mathbf{M}\cdot\nabla\mathbf{B}^0, \quad \mathbf{C} = \mathbf{M} \times \mathbf{B}^0. \tag{3}$$

These forces are conservative in the sense that they can be derived from a magnetic potential, expressed as a volume integral over the beam

$$\mathscr{W} = -\tfrac{1}{2}\int \mathbf{M}\cdot\mathbf{B}^0 \, dv. \tag{4}$$

The existence of this potential is important for the dynamics and stability of the beam. It means that for an autonomous system (i.e., no driving force) only a static buckling or divergence instability can occur. (Note that although these magnetic forces are of the follower type, they are still conservative.) Thus flutter type motions cannot occur for the linearized autonomous system.

In this problem eddy currents and associated forces are not treated explicitly, nor is magnetic hysteresis in the ferromagnetic (steel) beam included. Small eddy current induced damping is treated as a part of the overall damping in the beam. Non-linearities in the relation **M(B)** are also neglected. The non-linearities included in the analysis reflect the inhomogeneous nature of the magnetic field $\mathbf{B}^0$ and the magnetic force and couple (3). The magnetic field lines in the vicinity of the end of the beam are shown in Figure 3. It is clear that for beam tip motions of the order of the magnet spacing the magnetic forces depend in a non-linear manner on the tip displacement.

To determine the magnetization it is assumed that the beam is a wide plate. It is further assumed that locally the magnetic field $\mathbf{B}^0$ can be treated as uniform and that the dependence of **M** on the beam curvature is small. Under these assumptions it can be shown (see reference

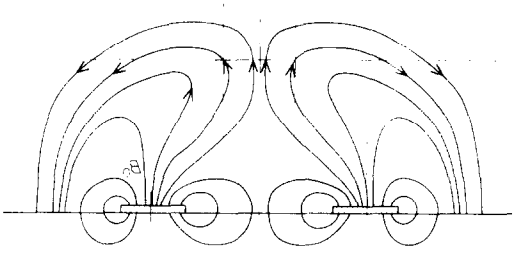

Figure 3. Magnetic field pattern in the vicinity of the beam tip.

[9]) that **M** is given by the expression

$$\mathbf{M} = \frac{\chi B_0(x, y)}{\mu_0}\left(\frac{\cos\beta}{\mu_r}\hat{\mathbf{n}} + \sin\beta\,\hat{\mathbf{a}}\right), \tag{5}$$

where $\hat{\mathbf{n}}$ and $\hat{\mathbf{a}}$ are unit vectors normal and tangent to the beam-plate (see Figure 4) and β is the local angle between the external field $\mathbf{B}^0$ and the plate normal $\hat{\mathbf{n}}$. $\mu_r = \chi + 1$ is the relative

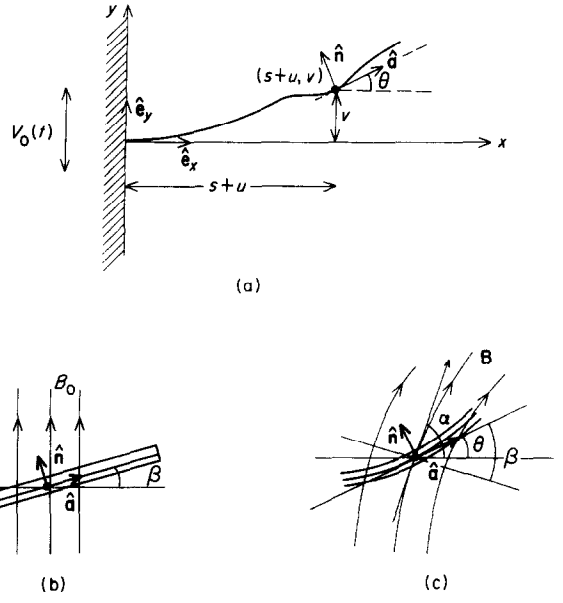

Figure 4. (a) Sketch of co-ordinate system used in the theoretical analysis; (b) beam element in a uniform magnetic field; (c) beam element in a non-uniform magnetic field.

permeability of the beam. The field shape B_0 is to be evaluated in terms of the local x, y co-ordinates of the plate neutral surface.

If the x, y components of B_0 are introduced, defined by $B_{0x} = B_0 \cos\alpha$ and $B_{0y} = B_0 \sin\alpha$, and the local slope of the beam with the x axis by θ, then one can rewrite equation (5), making use of the identity $\beta = \pi/2 + \theta - \alpha$. The magnetic energy potential then takes the form

$$\mathcal{W} = -\frac{\chi}{4\mu_0\mu_r}\int_0^L (B_1 + B_2 \sin 2\theta + B_3 \cos 2\theta)\,\mathrm{d}s, \tag{6a}$$

where

$$B_1 = (\mu_r + 1)(B_{0x}^2 + B_{0y}^2), \quad B_2 = 2(\mu_r - 1)\, B_{0x}B_{0y}, \quad B_3 = (\mu_r - 1)(B_{0x}^2 - B_{0y}^2). \tag{6b}$$

Here the integration is carried out over the original length of the beam and B_1, B_2 and B_3 are functions of the beam displacement $(u(s), v(s))$ since B_0 is evaluated at $x = s + u$, $y = v$ (see Figure 4(a)).

2.2. DISCRETE MODEL, A BUTTERFLY CATASTROPHE

An heuristic one dimensional theoretical model can be obtained by assuming that only the tip of the beam is magnetized and neglecting the effect of the couple **C** in equation (3).

If it is assumed that the magnetization at the tip lies primarily along the beam, or that $\mathbf{M} = [\chi/(\chi + 1)]\, B_{0x}\hat{\mathbf{a}}$, the effect of tip rotation being neglected, then the normal component of the total magnetic force on the tip is of the form

$$\mathscr{F}_y = \alpha B_{0x} \frac{\partial}{\partial x} B_{0y}, \tag{7}$$

where α includes the effects of χ and beam geometry. Using the fact that $\mathbf{B}^0$ is irrotational, i.e., $\nabla \times \mathbf{B}^0 = 0$, one can write

$$\mathscr{F}_y = -\partial \mathscr{W}/\partial y, \quad \mathscr{W} = -\tfrac{1}{2}\alpha B_{0x}^2, \tag{8}$$

where $\mathscr{W}$ is the magnetic potential energy.

If the magnets are symmetrically placed about the origin, the experimental data requires a non-linear force dependence on the tip displacement y of the type shown in Figure 5(a). The lower order terms in the Taylor expansion of $\mathscr{W}$ which will model the static bifurcation or buckling form a sixth order polynomial: i.e.,

$$\mathscr{W} = \tfrac{1}{2}ay^2 + \tfrac{1}{4}dy^4 + \tfrac{1}{6}cy^6. \tag{9}$$

If a single mode approximation is made for the beam deformation, the elastic energy has the form

$$\mathscr{V} = \tfrac{1}{2}ky^2 + (\text{higher order terms}). \tag{10}$$

Measurements indicate that the non-linear elastic forces are small even for the large displacements of the beam tip observed in the experiments; moreover, non-linear elastic forces are not required to explain the experimental data. Thus we choose as a potential for the elastic and magnetic forces,

$$\mathscr{V}_1 = \mathscr{V} + \mathscr{W} = \tfrac{1}{6}cy^6 + \tfrac{1}{4}dy^4 + \tfrac{1}{2}(k + a)\, y^2. \tag{11}$$

Study of the critical points of this potential shows that there may be one, three, or five fixed points for the tip displacement, as the experimental data suggests. Figure 5 shows the equilibrium position of the beam tip as a function of magnet separation. In the actual experiment exact conditions of symmetry cannot be obtained so that the experimentally determined curve in Figure 6 represents one "unfolding" of the above potential $\mathscr{V} + \mathscr{W}$. As one decreases the magnet separation distance (vertical axis in Figures 5(b) and 6) the number of equilibrium points changes from one to five to three. This particular unfolding is in fact a *butterfly catastrophe* [10]. The path shown in Figure 5(c) represents only one possible variation of parameter in the problem. Results from catastrophe theory [10] assert that in general four parameters are required to describe all the changes in the number of equilibrium

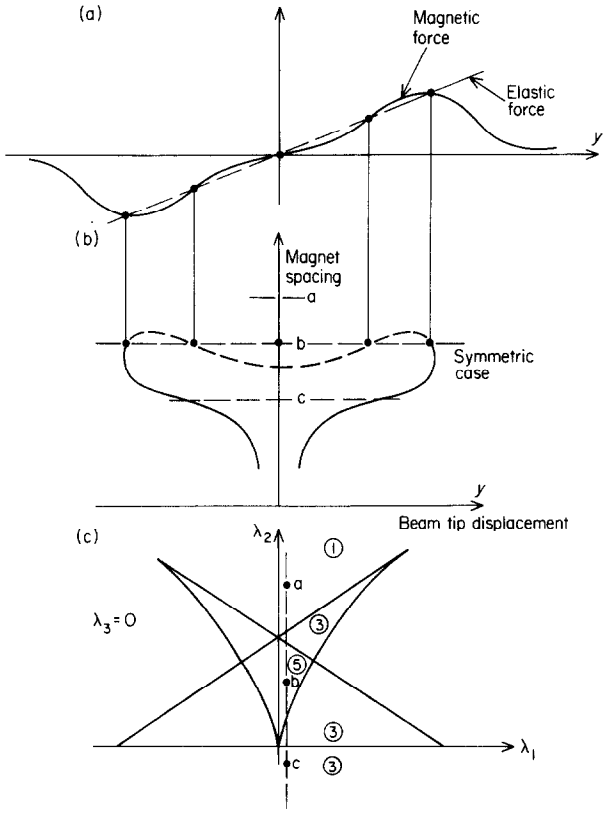

Figure 5. (a) Magnetic and elastic forces as a function of tip displacement, y; (b) equilibrium positions as a function of magnet spacing; (c) "butterfly" catastrophe set showing number of equilibrium points as a function of magnetic spacing λ_2 and imperfection λ_1.

positions for a sixth order potential. Thus a more general form for $\mathscr{V}_1$ is

$$\mathscr{V}_1 = \tfrac{1}{6}y^6 + \tfrac{1}{4}\lambda_4 y^4 + \tfrac{1}{3}\lambda_3 y^3 + \tfrac{1}{2}\lambda_2 y^2 + \lambda_1 y. \tag{12}$$

In the problem here, λ_1 and λ_3 represent departures from symmetry (unequal magnet spacing or magnet strength), $\lambda_4 < 0$ is related to the magnetic forces, and combined magnetic and elastic linear force constants are contained in λ_2. The results in Figure 6 can be explained by examining the catastrophe set in the $\lambda_2 - \lambda_1$ plane for $\lambda_3 = 0$ and $\lambda_4 < 0$, as shown in Figure 5(c). This diagram gives curves across which the number of equilibrium points change. We believe the data in Figure 6 to be consistent with a vertical parameter path shown by the dotted line, where a small imperfection λ_1 is present. This path through the butterfly catastrophe explains the jumps from one to three to five to three equilibrium positions.

2.3. A CONTINUUM MODEL

In this section the derivation of a continuum model for a non-linear elastic cantilever in a non-linear, non-uniform magnetic field is sketched out. Inextensibility along the beam is assumed and subsequently attention is restricted to relatively small lateral motions, thus reducing the elastic forces to the usual linear ones while retaining the non-linear magnetic forces.

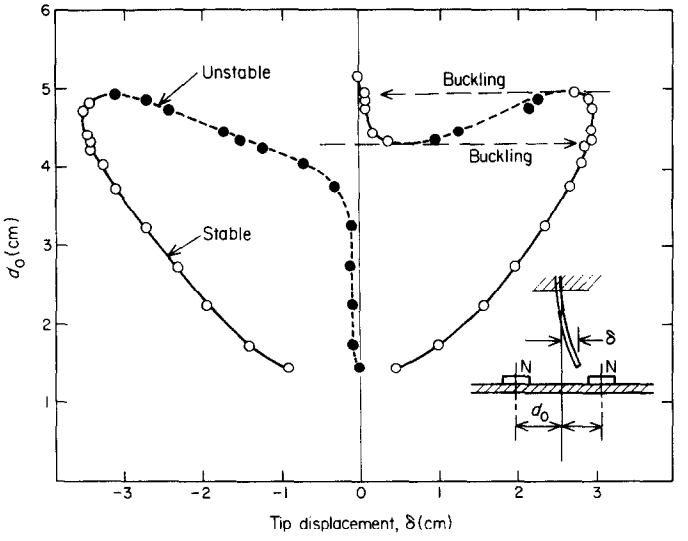

Figure 6. Experimental buckling curve showing equilibrium beam tip positions versus magnet spacing d_0.

Consider the Lagrangian

$$\mathscr{L} = \mathscr{T} - (\mathscr{V} + \mathscr{W}), \tag{13}$$

where $\mathscr{T}$, $\mathscr{V}$ and $\mathscr{W}$ are kinetic, elastic and magnetic energies respectively. Using the coordinate system of Figure 4(a) again, where the elastic displacements $u(s)$, $v(s)$ and $\theta(s)$ are referred to the centroid of cross-section, one finds that the slope and displacements are related by

$$\tan\theta = v'/(1 + u'), \tag{14}$$

and inextensibility implies that

$$(1 + u')^2 + (v')^2 = 1, \tag{15}$$

where $(\,)' \triangleq (\partial/\partial s)$. In this derivation the treatment of Beck's column due to Crespo da Silva [11] is followed. To cope with the constraint (15) an undetermined Lagrange multiplier $T(s, t)$ is introduced, so that, with use of the magnetic potential (6), the statement of Hamilton's principle becomes

$$\delta \int_{t_1}^{t_2} \int_0^L \{\tfrac{1}{2}m[\dot{u}^2 + (\dot{v} + \dot{V}_0)^2] - \tfrac{1}{2}D(\theta')^2 + \psi + \tfrac{1}{2}T[1 - (1 + u')^2 - (v')^2]\} \times \mathrm{d}s\,\mathrm{d}t = 0, \tag{16}$$

where

$$\psi = -(\chi\Delta/4\mu_0\mu_r)(B_1 + B_2 \sin 2\theta + B_3 \cos 2\theta). \tag{17}$$

The beam thickness is denoted by Δ and B_1, B_2 and B_3 are as given in equations (6b). D is the elastic stiffness constant for the beam. $V_0(t)$ is the motion of the reference platform to which the beam is attached. Using the fact that the variation

$$\delta\theta = -v'\delta u' + (1 + u')\,\delta v', \tag{18}$$

from equations (14) and (15), one obtains two partial differential equations of motion and the boundary conditions,

$$\partial\psi/\partial v - G' = m(\ddot{v} + \ddot{V}_0), \quad \partial\psi/\partial u + H' = m\ddot{u}, \quad [-D\theta'\delta\theta + G\delta v - H\delta u]_0^L = 0, \qquad (19a\text{–}c)$$

where

$$G = D\theta''(1 + u') + (\partial\psi/\partial\theta)(1 + u') - Tv', \quad H = D\theta''v' + (\partial\psi/\partial\theta)\,v' + T(1 + u').$$

The cantilevered boundary conditions imply that

$$u(0, t) = v(0, t) = \theta(0, t) = 0, \quad G(L, t) = H(L, t) = \theta'(L, t) = 0.$$

First one can note that the general formulation of equations (19) enables a number of special cases to be recovered. The static buckling of an inextensible beam plate in a uniform magnetic field can be found by setting

$$\ddot{u} = \ddot{v} = \ddot{V}_0 = 0, \quad \partial\psi/\partial u = \partial\psi/\partial v = 0.$$

This results in the equations

$$D\theta'' + \partial\psi/\partial\theta = 0, \quad T = 0,$$

or, upon substituting for ψ from equation (17),

$$D\theta'' + (\chi\Delta/2\mu_0\mu_r)(B_2 \cos 2\theta - B_3 \sin 2\theta) = 0.$$

For a transverse magnetic field this leads to an elastic type buckling problem (see reference [9]);

$$D\theta'' + [\chi^2\Delta/2\mu_0(\chi + 1)]\, B_{0y}^2 \sin 2\theta = 0. \qquad (20)$$

Since the goal is to obtain a theoretical model which exhibits all the qualitatively important features of the experimental model, only those non-linearities which are essential need be retained. In particular we have observed experimentally that the elastic behavior of the beam is almost linear under non-magnetic forces even for tip deflections of the order of 20–30% of the length. Therefore one can drop all non-linearities in the slope and curvature, e.g., θ', θ'', θ^2, etc., while retaining non-linear terms in the displacement v. Under these assumptions θ can be replaced by v' and equations (19a, b) become

$$\frac{\partial\psi}{\partial v} - Dv'''' - \frac{\partial\psi'}{\partial\theta} + (Tv')' = m(\ddot{v} + \ddot{V}_0), \quad T(s) = T(L) - \int_0^s \frac{\partial\psi}{\partial u}\,ds, \qquad (21a, b)$$

along with the boundary conditions

$$v = v' = 0 \text{ at } x = 0,$$
$$v'' = 0,\ T = 0,\ Dv''' + \partial\psi/\partial\theta = 0, \text{ at } x = L.$$

Equation (21a) can be interpreted in terms of the physics if one recognizes that the magnetic force and couple per unit length along the beam are given by

$$(\mathscr{F}_x, \mathscr{F}_y) = (\partial\psi/\partial u, \partial\psi/\partial v), \qquad C = \partial\psi/\partial\theta.$$

Thus the Lagrange multiplier T is just the tension in the beam created by the axial magnetic force and the term $(Tv')'$ represents the restoring force on the beam due to this tension. The body couple gradient C' appearing in the equation is precisely that required for the moment

equilibrium about the z axis normal to the x-y plane. By using equation (17) it is easy to show that in a linear approximation and for $B_{0y} \simeq 0$, $C = \kappa\theta \approx \kappa v'$, where $\kappa > 0$ is related to the external magnetic field. Equation (21) does not include damping forces, which will be considered in the next section.

3. REDUCTION OF THE MODEL TO AN ORDINARY DIFFERENTIAL EQUATION

3.1. GALERKIN'S METHOD

In Galerkin's method a suitable set of (orthogonal) basis functions $\phi_j(x)$, which satisfy the boundary conditions, is chosen and the unknown displacement, v, expressed as

$$v(x, t) = \sum_{j=1}^{\infty} a_j(t)\, \phi_j(x). \tag{22}$$

A typical choice for the ϕ_j in vibration problems are the normal modes of the associated linear problem. One then substitutes expression (22) into the equation of motion and takes the inner product (i.e., integrates over the (normalized) beam length) with $\phi_k(x)$, $k = 1, 2, 3, \ldots$, thus obtaining an infinite set of second order ordinary differential equations (ODE's) for the unknown modal coefficients $a_j(t)$.

It is well known that modal coupling can occur in certain problems, leading to flutter instabilities (cf., reference [12]); thus in general one might have to consider pairs of modes. The form of equation (21), however, is such that, given a suitable choice of basis functions (normal modes), the modes remain linearly uncoupled in the absence of external force ($V_0 = 0$), and hence the "first" mode loses stability independently as a simple eigenvalue passes through zero. Here the instability is divergence rather than flutter. See Appendix A for further details.

Since it is observed that the lowest mode is dominant in the motion of interest here, a single mode approximation

$$v(x, t) = a(t)\, \phi(x), \tag{23}$$

can be chosen where $\phi(x)$ is required to satisfy

$$\phi(0) = \phi'(0) = \phi''(L) = 0, \qquad D\phi'''(L) + \kappa\phi'(L) = 0, \qquad \int_0^L \phi^2 \, dx = 1.$$

The resulting differential equation for $a(t)$ is

$$m\ddot{a} + \left\{ \int_0^L (\kappa + T)(\phi')^2 \, dx + D \int_0^L (\phi'')^2 \, dx \right\} a = \int_0^L \mathscr{F}_y \phi \, dx - m\ddot{V}_0 \int_0^L \phi \, dx. \tag{24}$$

It must be remembered that κ, T and $\mathscr{F}_y$ all depend on B_{0x} and B_{0y}, which themselves depend on $a(t)$. To proceed further one can assume that $\mathbf{B}^0$ acts primarily at the beam's tip; a study of the magnetic field indicates that this is quite reasonable. Thus one may write

$$\mathscr{F}_y = F_y \delta(x - L), \qquad \mathscr{F}_x = F_x \delta(x - L), \qquad \kappa = K\delta(x - L). \tag{25}$$

These assumptions then lead to

$$T = T_0 = F_x,$$

$$m\ddot{a} + \left\{ D \int_0^L (\phi'')^2 \, dx + K\phi'(L)^2 + F_x(a) \int_0^L (\phi')^2 \, dx \right\} a - F_y(a)\, \phi(L) = m\ddot{V}_0 \int_0^L \phi \, dx. \tag{26}$$

The effective stiffness of this model is the bracketed term, which contains both elastic and

magnetic contributions. In fact one could hinge the beam and set $\phi'' \equiv 0$ and still have a restoring force due to the magnetic end couple and magnetic tension.

To complete the model one can assume the following forms for the functions $F_x(a)$ and $F_y(a)$, which appear to be consistent with the physics,

$$F_x = F_0, \text{ a constant}, \quad F_y = [m/\phi(L)](\alpha_1 a + \beta a^3 + \eta a^5 + \ldots), \tag{27}$$

and add a damping term. Here α_1, β and η are related to the local magnetic field at the beam tip and field gradients.

If one assumes that $V_0(t) = [A_0/\int_0^L \phi \, dx] \cos \Omega t$, then the equation of motion for the modal amplitude $a(t)$ takes the form

$$\ddot{a} + \delta \dot{a} - \alpha a + \beta a^3 + \eta a^5 = \Omega^2 A_0 \cos \Omega t, \tag{28}$$

where

$$\alpha = \alpha_1 - \frac{1}{m}\left\{D \int_0^L (\phi'')^2 \, dx + \kappa \phi'(L)^2 + F_x \int_0^L (\phi')^2 \, dx\right\}.$$

In the absence of external forcing ($A_0 = 0$) the static bifurcation problem corresponding to equation (28) has precisely the potential energy function of equation (11), with $\alpha = -(k + a)$, $\beta = d$ and $\eta = c$. If the static problem has only three equilibrium points the fifth order term may be dropped, since it does not alter the qualitative behavior, and equation (28) may then be non-dimensionalized to the form

$$\ddot{A} + \gamma \dot{A} - \tfrac{1}{2}(1 - A^2) A = f \cos \omega t \tag{29}$$

in which the characteristic time and distance, $1/\omega_0 = 1/(2\alpha)^{1/2}$ and $a_0 = (\alpha/\beta)^{1/2}$, are used, ω_0 representing the natural frequency about the buckled position a_0. Both α and β can be derived experimentally, as can the damping γ. The following non-dimensional groups are sufficient to characterize the three equilibrium state problem:

$$\gamma = \delta/\omega_0, \qquad f = \Omega^2 A_0/\omega_0^2 a_0, \qquad \omega = \Omega/\omega_0. \tag{30}$$

3.2. COMMENTS ON THE REDUCTION OF DIMENSION

Equation (29) might appear to be a crude model, since in its derivation approximations have been made both in the continuum formulation and in the single mode Galerkin representation. However, the latter approximation need cause no loss whatever in *qualitative* information, for the following reason. In an earlier paper [12], Holmes showed how the Center Manifold Theorem could be used to reduce locally a high dimensional problem, near a bifurcation point, to one of low dimension. The approach was later extended [13] to the full partial differential equation. The Center Manifold Theorem states that near a bifurcation point one can restrict attention to an invariant subsystem of dimension equal to the number of eigenvalues involved in the bifurcation. This is essentially equivalent to ignoring all but the most unstable mode(s) of vibration, and the center manifold can be seen as a curved subspace locally tangent to the eigenspace of this mode. Technical details can be found in references [14–16].

Further comments on the application of bifurcation theory and invariant manifolds to the reduction of the partial differential equations (21a, b) to the ordinary differential equation (29) may be found in Appendix A.

4. ANALYSIS OF THE SINGLE MODE MODEL

In this section theoretical results on the behavior of equation (29) are outlined. This work has been reported at length elsewhere [2–4].

In reference [2] it is proved that an equation equivalent to equation (29) is *globally stable* in the sense that after sufficient time all solutions enter and remain within a bounded set in the $(a, \dot{a})$ state space: thus the system (29) always has at least one *attractor* [17]. One can rewrite it as an autonomous system on $\mathbf{R}^2 \times \mathbf{S}^1$, with $A_1 = A$, $A_2 = \dot{A}$ and $t = \theta$ as

$$\dot{A}_1 = A_2, \qquad \dot{A}_2 = \tfrac{1}{2}A_1(1 - A_1^2) - \gamma A_2 + f\cos\omega\theta, \qquad \dot{\theta} = 1, \tag{31}$$

and consider the Poincaré map $P_f : \Sigma \to \Sigma$, on the cross-section $\Sigma = \{(x, y, \theta) \in \mathbf{R}^2 \times \mathbf{S}^1 \mid \theta = 0, 2\pi, \dots\}$, defined by solutions of system (31) (cf. reference [17]). One can now study the orbit structure of P_f (and hence of system (31)) as the force amplitude parameter, f, increases.

First consider the case $f = 0$. Here all cross-sections are identical for all $\theta \in [0, 2\pi]$. The Poincaré map thus has a structure identical to that of the vector field of the autonomous two dimensional system,

$$\dot{A}_1 = A_2, \qquad \dot{A}_2 = \tfrac{1}{2}A_1(1 - A_1^2) - \gamma A_2, \tag{32}$$

in the sense that the stable and unstable *manifolds* $M^s(s)$, $M^u(s)$ [17] of the saddle (0, 0) of the Poincaré map are curves identical to the stable and unstable *seperatrices* of (0, 0) for the vector field. However, one must recall that an orbit of the map under iteration of P_f is a sequence of *points* a, $P_f(a)$, $P_f^2(a), \dots, P_f^n(a), \dots$, and not a curve, as in the case of vector fields [17]. Each manifold is invariant in the sense that an orbit starting on it remains on it under iteration of P_f. It is easy to check [2] that the Poincaré map for $f = 0$ is (globally) *structurally stable* and one can thus conclude that for $f \neq 0$, small, the topological type of P_f will be identical to that for $f = 0$. This is confirmed by analog computer analysis, as described in reference [2]. Thus, for small f, P_f has a saddle and two stable sinks, corresponding to the two attracting and one repelling closed orbits of the differential equation (31) (see Figure 7(a)).

As f increases it is possible to prove, by using the method of Melnikov [18], that the stable and unstable manifolds of the saddle point approach and ultimately intersect, giving rise

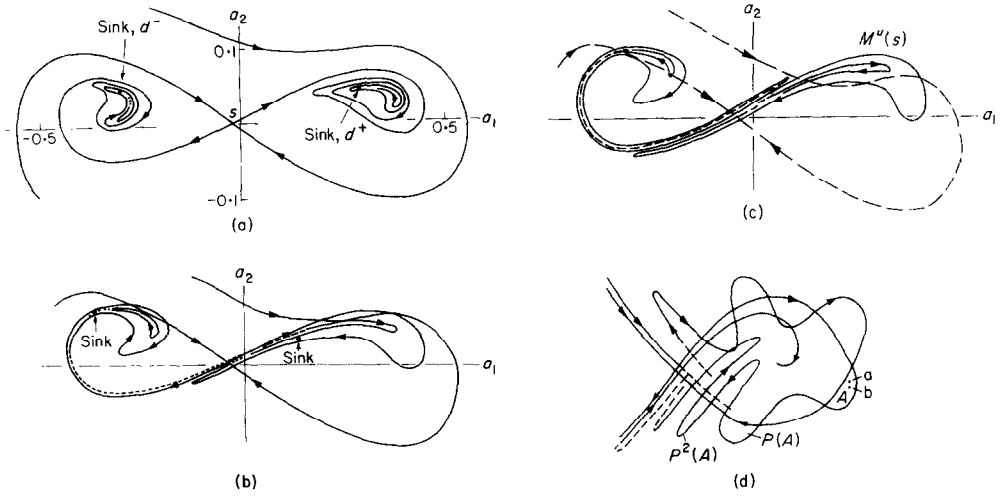

Figure 7. Analog computer plots of the Poincaré map of equation (29). (a) $f < f_1$; (b) $f_1 < f < f_2$; (c) $f > f_2$; (d) schematic structure of one "lobe" (from reference [2]).

to infinitely many homoclinic points [17]. (A paper which describes these methods and draws together other relevant material is to appear [19], but for completeness we sketch the method here in Appendix B.) The stable and unstable manifolds of the saddle of P_f wind more and more violently and ultimately intersect (see Figure 7(b)). In reference [2] it is shown that these intersections occur at a critical force value $f = f_1$. In this case, for $\gamma, f \ll 1$, f_1 can be estimated as

$$f_1 \approx (\sqrt{2}\gamma/3\pi\omega)\sinh(\pi\omega/\sqrt{2}). \tag{33}$$

It follows from the work of Smale [20] (cf. reference [21]), that, for $f > f_1$, P_f possesses a complicated invariant set Ω_h near the homoclinic points. This is best described in terms of its effect on solutions starting close together. Consider two points a, b lying in one of the loops bounded by stable and unstable manifolds shown in Figure 7(d). Under iteration of P_f the loop A is mapped into $P_f(A)$, $P_f^2(A)$, etc. Note that the loop is stretched and thus most pairs of arbitrarily close points are separated dramatically as P_f is iterated. In the case of the system (31), points cannot escape to infinity on account of the global stability, and $P_f^n(A)$ as $n \to \infty$ is stretched and wound into the other lobe. In doing so $P_f^n(A)$ intersects the infinite windings of the manifolds in the left lobe with the result that, for sufficiently large n, no matter how close a and b are, $P_f^n(a)$ and $P_f^n(b)$ lie on opposite sides of the stable manifold $M^s(s)$ and their fates are thus quite different (cf. Figure 8, below).

However, Ω_h also contains a countably infinite set of periodic points of all periods and an uncountable set of dense non-periodic orbits. Now if a and b happen to lie on periodic orbits of the same period their iterates will not diverge. However, since the periodic orbits are not attractors, but are all of saddle type, it is very unlikely that the physical system will follow a periodic orbit. It may, however, remain near one for a long time and then diverge relatively suddenly. The behavior of orbits originating in or entering the neighborhood of Ω_h therefore appears unpredictable and chaotic.

Now for f slightly greater than f_1, the two stable sinks d^+, d^- still exist (Figure 7(b)), but the presence of the homoclinic intersections causes solutions to wander erratically back and forth for a time before approaching one of the sinks. Experimental observations of this are discussed in section 5. Similar sensitive dependence on initial conditions has been noted in other mechanical systems—for a discussion of determination of the resulting highly irregular domains of stability see reference [22].

As f continues to increase, the analog computations of reference [2] show that the fixed points d^+, d^-, of Figure 7(a) bifurcate to sinks of period 2 and then of period 4. It is possible that further bifurcations, to periods 8, 16, 32, ... also occur but they are difficult to detect with reliability. In any case after a second critical value of f, f_2, successive iterates of P_f are no longer attracted to a clearly periodic orbit and they appear to wander chaotically back and forth across Σ. Figure 7(c) indicates that this wandering is in fact ordered in the sense that the orbits rapidly converge on and appear to remain on a one dimensional curve which appears identical to the unstable manifold of the saddle. Computations of the power spectrum for some 50 000 samples (12 000 cycles of the forcing function) clearly suggest non-periodic behavior [2] (cf. also reference [3]). In reference [2] it is suggested that for $f \in (1{\cdot}08, 2{\cdot}45)$ P_f has a non-periodic *strange attractor*. In Figure 2 a typical time history $a(t)$ of equation (31) has been shown. The solution appears to be thrown back and forth chaotically but this motion is in fact completely determined by the stable and unstable manifolds $M^s(s)$, $M^u(s)$ of the saddle point s of P_f, which wind back and forth as indicated in Figure 7(c), intersecting each other infinitely many times in the process.

In reference [2] the structure of this strange attractor, S, is analyzed in some detail; here one may merely note that, while solutions converge relatively rapidly to S, they move on S in an ergodic manner so that the solution $x(t)$ appears to be chaotic, and has a continuous

power spectrum, indicating that energy is present at all frequencies. For related work in non-linear oscillations of electrical circuits see the papers by Ueda *et al.* [23, 24].

If there are five equilibria, two saddles and three sinks, in the unforced problem, then the structure discussed above is repeated as indicated in Figure 8. The effect here is that orbits move irregularly between *three* states: oscillation about the central point alternating erratically with oscillation about the two extreme points. Global stability again ensures that there

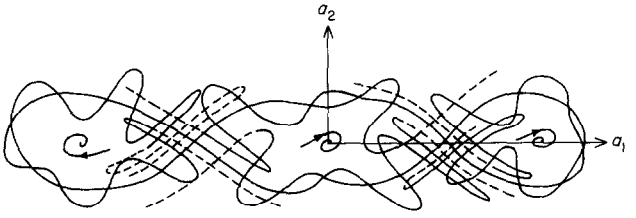

Figure 8. The Poincaré map for the five equilibria case.

are no orbits escaping to infinity. As outlined in section 5, this case may in fact be more important in physical applications.

We now turn to the experimental results, which we shall interpret in the light of the analysis outlined in this section.

5. EXPERIMENTAL RESULTS

5.1. DESCRIPTION OF EXPERIMENTAL MODEL

The apparatus consisted of a cantilevered beam, permanent magnets, a vibration shaker and strain gage recording devices as shown in Figure 1. The beam was made from a steel rule 0·23 mm (0·009 inch) thick, 9·5 mm ($\frac{3}{8}$ inch) wide, and 18·8 cm (7·4 inch) long. The beam was clamped vertically at one end and suspended at the other end between two rare earth permanent magnets. The 2·54 cm (1 inch) diameter magnets had a 0·18 Tesla field normal to the magnet face in air. The magnets were secured to a steel base. This base and the beam clamp were attached to a wood plate which was driven by an electromagnetic shaker. The resulting acceleration was transverse to the beam and the frequency of oscillation was varied from 2–20 Hz, with a maximum amplitude of about 1 cm (0·39 inch).

A linear variable differential transformer was attached to the shaker platform in order to measure the forced vibration amplitude. Strain gages were attached to the base of the beam near the clamped end to measure the beam motion. Data was recorded on both a strip chart recorder and an oscilloscope.

Data from the strip chart recorder was later digitized and recorded on digital computer cards for spectral analysis, accomplished by using a fast Fourier transform algorithm.

5.2. EXPERIMENTAL RESULTS

When the magnets are placed far from the beam tip, the beam oscillates around the straight position with natural frequencies of 4·6, 26·6 and 73·6 Hz for the lowest three modes. The measured frequency ratios of these modes are slightly higher than the theoretical values due to the presence of strain gage leads near the clamped base, which provide some stiffening of the first mode. As the magnets are moved toward the ferromagnetic beam, two and then four

new equilibrium positions appear as shown in Figures 5 and 6, so that three stable equilibrium positions are possible. With further decrease in magnet separation three equilibrium positions coalesce into one so that three remain. The straight beam or center position becomes unstable and the beam bends either to one side or the other.

Most of the experiments were carried out for the three equilibrium case (point "c" in Figure 5). The post-buckled beam had a static tip deflection of 1·68 cm from the unbent beam position. The lowest natural frequency about these new equilibrium positions was 9·3 Hz. The clamped end of the beam was attached to an electromagnetic vibrator. For small motions of the vibrator, the beam exhibited oscillations about one or the other stable equilibrium point, but for larger amplitudes the beam would jump from motion about one equilibrium position to motion about the other. Some of these motions were periodic. However for what appear to be a dense set of frequency-amplitude parameters the beam exhibited chaotic-like motions even though the driving amplitude was highly sinusoidal and of constant amplitude. Traces of these motions, as recorded by the strain gages, are shown in Figures 2 and 9, and later in Figure 13. Once the beam entered into this state of motion for a

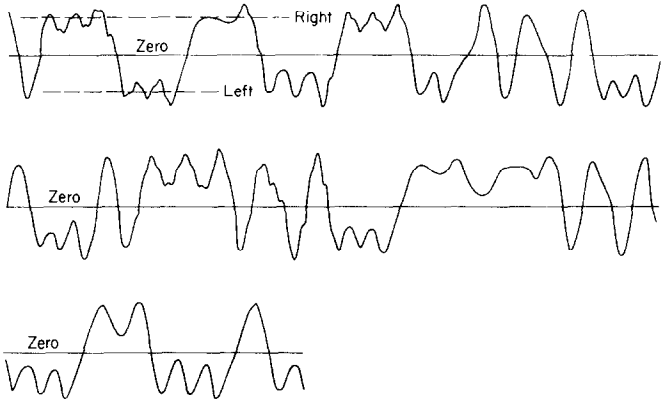

Figure 9. Bending strain versus time record for strange attractor vibrations used in discrete Fourier spectrum in Figures 10(a), (b).

particular shaker frequency and amplitude, the motion would remain chaotic. Such motions were observed for over an hour, without the beam settling into a steady state motion. The initial condition for each run was a given displacement of the beam greater than the non-zero equilibrium positions. If the resulting motion appeared chaotic and continued for more than a minute the corresponding point in the frequency-forcing amplitude plane was labeled "chaotic". Below this "chaotic" forcing amplitude limit motions might exhibit chaotic behavior initially but would settle into a periodic mode within one minute.

Besides time domain records of these motions, a frequency analysis of several time records were made. This was done by digitizing the strip chart data of Figure 9 and using a fast Fourier transform algorithm to obtain frequency spectra. While many such spectra would be required to establish reliable statistics for this motion, the few sample spectra obtained show similar characteristics (see Figures 10(a), (b)). Of immediate importance is the broad frequency content for a single frequency input. While conventional non-linear analysis might lead one to expect harmonics or even subharmonics of the driving frequency, the strange attractor motions here seem to generate a continuous spectrum of frequencies associated with the non-periodic motion.

Another experimental measure of the chaotic nature of this motion is the distribution of times spent on either side of the zero position, and measurements of times between

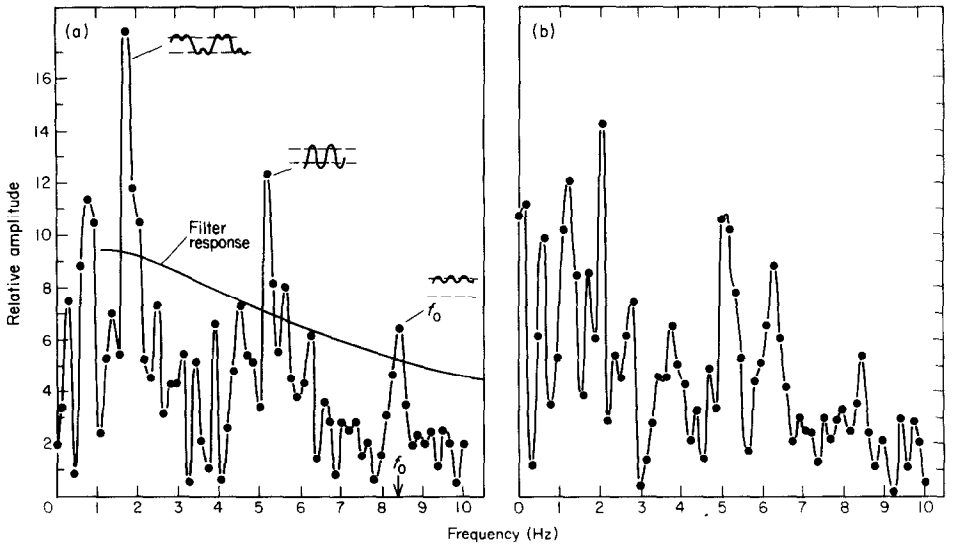

Figure 10. Discrete Fourier transform (FFT) of 128 digitized data points for two consecutive time records (see Figure 9).

consecutive zero crossings of the displacement showed a broad distribution of times greater than the forcing period.

While various qualitative analyses have demonstrated the existence of strange motions in deterministic non-linear systems, there is no theory at present to predict for what range of parameters these chaotic motions will occur. The engineer would like a critical parameter or

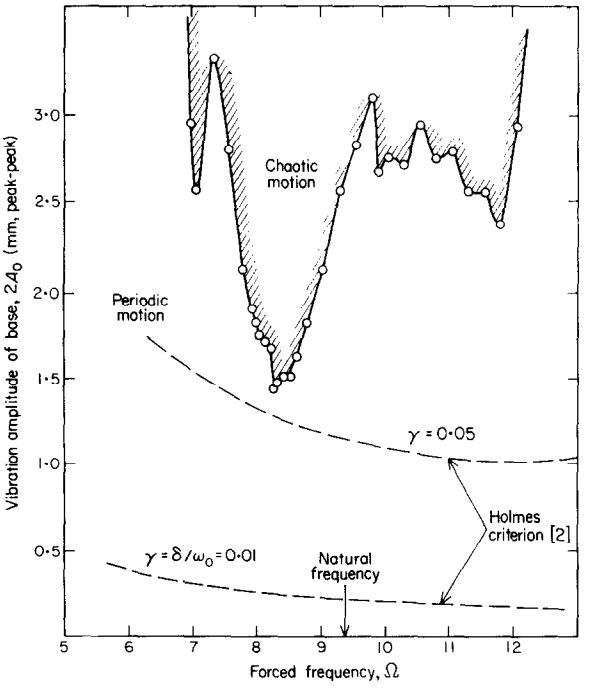

Figure 11. Experimental and theoretical criteria for chaotic motion in the forcing frequency–amplitude plane. $\partial v(L) = 3{\cdot}35$ cm; $\omega_0/2\pi = 9{\cdot}4$ Hz; $\gamma = 0{\cdot}0036$.

equivalent of a critical "Reynolds number" for which these motions might occur in his physical system. With our experimental model, a set of parameters in driving frequency and amplitude was obtained for which these motions would occur, as shown in Figure 11 for the three equilibrium position case. The chaotic motion regions seem to resemble the unstable regions in the frequency-load plane for the Mathieu equation or parametric oscillations.

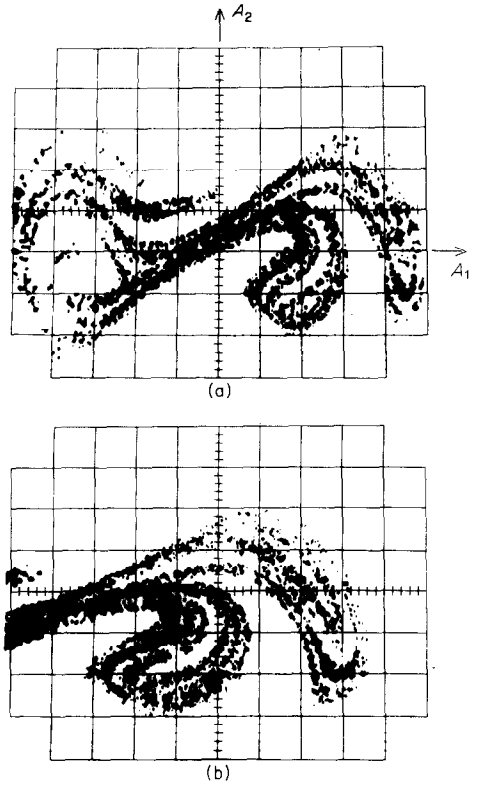

Figure 12. (a) Typical experimental Poincaré section of a strange attracting set for a beam with damping ratio $\gamma = 0{\cdot}026$, forcing frequency 8·5 Hz, and forcing amplitude 3 mm, peak to peak; (b) enlargement of the right-hand "lobe" in part (a).

The data for Figure 11 was obtained by fixing the frequency and increasing the amplitude of the shaker. The theoretical condition for the creation of homoclinic orbits derived by Holmes [2], equation (33), is shown for two different damping ratios. It represents a lower bound for *transient* chaotic behavior but not for sustained chaotic motions, at least for the range of non-dimensional parameters used in these experiments. The analysis in reference [2], sketched here in section 4, shows that homoclinic orbits are generally created at lower force levels than that at which the non-periodic attractor appears. In fact in the work reported in reference [2] it was found that the homoclinic orbits of the Poincaré map coexist with two stable sinks, representing periodic motions for a considerable force range. However, the existence of the homoclinic orbits implies that solutions might behave in an apparently chaotic manner for a time before finally approaching a periodic orbit, and this is exactly what is observed in the experiments.

While the magnetic beam experiments reported here exhibit strange attractor results qualitatively similar to those of reference [2], it should be noted that the non-dimensional

parameters differ. Typical values for each are as follows:

reference [2]: $\gamma = 0{\cdot}045, \quad f = 0{\cdot}28, \quad \omega = 0{\cdot}84;$

magnetic beam: $\gamma = 0{\cdot}0036, \quad f = 0{\cdot}035, \quad \omega = 0{\cdot}89.$

In the analog computer experiments [2], the attracting set in the Poincaré map was shown to be a curve apparently identified with the unstable manifold of the saddle point. A similar set was obtained experimentally for the magnetoelastic strange attractor and is shown in Figure 12. An electronic differentiator was built so that the phase plane motion of strain versus strain rate could be displayed on an oscilloscope. Further, by controlling the scope trace brightness to intensity briefly at a given phase angle of the driving motion an experimental Poincaré map was obtained. The beam damping for the data in Figure 12 ($\gamma = 0{\cdot}026$) was higher than that for the data of the other figures ($\gamma = 0{\cdot}0036$). Figure 12 also indicates that the motion in the Poincaré plane is confined to a curve which folds back on itself many times. We believe this to be the first "picture" of a strange attracting set for a physical system, other than those produced by computing machines.

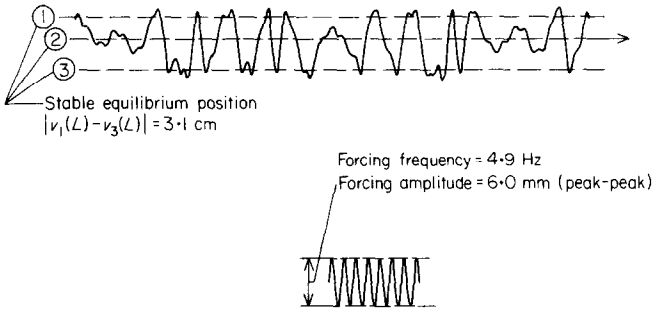

Figure 13. "Butterfly" strange attractor vibrations for the case of five static equilibrium positions (three stable points).

Finally we have obtained some preliminary evidence for strange attractor motions for the five equilibrium position cases as shown in Figure 13. Here the static condition corresponds to region *b* in the butterfly catastrophe set in Figure 5(b). The beam thus has three stable static positions and when excited with large enough amplitude, jumps from one of these three positions to another, as shown in Figure 13.

6. CONCLUSIONS

In this paper we have presented a general approach to the forced vibrations of non-linear structures in non-uniform magnetic fields, taking as a specific example the case of a cantilever, inertially excited and buckled between two magnets. The Lagrangian formulation of section 2 allows more general problems to be tackled in a similar manner. In the present case, arguing from both experimental and theoretical stand points, we have shown that non-linear elastic forces and the effects of the distributed magnetic field can both be neglected and we have studied the relatively simple partial differential equation (21). This equation has been further simplified by taking a single degree of freedom Galerkin approximation, and we have indicated why this drastic simplification can be expected to yield reasonable results.

The simple forced non-linear oscillator equation (29) thus obtained has been studied elsewhere [2–4] and we have briefly outlined these results in section 4. Finally we have

demonstrated that our experimental findings are in excellent qualitative agreement with the theoretical predictions.

This is, we believe, the first situation in which a reasonable case has been made for the existence of a strange attractor in a physically interesting problem and as such should be of interest both to mathematicians and engineers, since it demonstrates that great care must be taken in studying every deterministic problem *if it is non-linear*. As shown in reference [2], classical techniques, such as K–B averaging, in principle completely fail to detect the strange attractor motions of equation (29), and without an adequate (qualitative) topological understanding of the orbit structure, numerical results would be equally useless.

In his classic paper of 1963 [1] Lorenz showed how a drastic Galerkin truncation of the partial differential equations describing convective heat transport led to a set of three first order equations with chaotic dynamics. It is generally accepted that this truncation makes application to fluid dynamical problems such as turbulence problematical. In fact recent work on a 14 mode model [25] has given somewhat different results. In the present work we believe that, while our truncation to one mode is equally drastic, we have not lost any qualitative information, mainly because in this structural vibration problem the modes remain almost uncoupled.

In closing it should be mentioned that similar non-periodic, chaotic motions have been observed for a magnetically levitated rigid body, and that such motions may therefore be important in stability studies of magnetically levitated transportation systems [26]. There is also some evidence for their occurrence in conventional wheel-rail tracked vehicles.

ACKNOWLEDGEMENT

This research was supported in part by a grant from the National Science Foundation, Engineering Mechanics Division, Grant No. Eng 76–23627.

REFERENCES

1. E. N. LORENZ 1963 *Journal of the Atmospheric Sciences* **20**, 130–141. Deterministic nonperiodic flow.
2. P. J. HOLMES 1979 (to appear) *Philosophical Transactions of the Royal Society (London)*. A nonlinear oscillator with a strange attractor.
3. P. J. HOLMES 1977 *Applied Mathematical Modelling* **1**, 362–366. Strange phenomena in dynamical systems and their physical implications.
4. P. J. HOLMES and J. E. MARSDEN 1978 *Proceedings of the New York Academy of Sciences Meeting on Bifurcation Theory in the Scientific Disciplines, New York. 26 October–1 November* 1977 **316**, 608–622. Qualitative techniques for the bifurcation analysis of complex systems.
5. A. E. COOK and P. H. ROBERTS 1970 *Proceedings of the Cambridge Philosophical Society* **68**, 547–569. The Rikitake two-disc dynamo system.
6. K. A. ROBBIN 1976 *Proceedings of the National Academy of Sciences of the U.S.A.* **73**, 4297–4301. A moment equation description of magnetic reversals in the earth.
7. F. C. MOON and Y.-H. PAO 1968 *Journal of Applied Mechanics* **35**, 53–58. Magnetoelastic buckling of a thin plate.
8. F. C. MOON and Y.-H. PAO 1969 *Journal of Applied Mechanics* **36**, 92–100. Vibration and dynamic instability of a beam-plate in a transverse magnetic field.
9. F. C. MOON 1978 in *Mechanics Today* **4** (S. Nemat-Nasser Editor). Chapter V, Problems in magneto-solid mechanics.
10. T. POSTON and I. STEWART 1978 *Catastrophe Theory and its Applications*. London: Pitman.
11. M. R. M. CRESPO DA SILVA 1977 *Department of Engineering Science Report No. ES* 77–128, *University of Cincinnati*. Transverse non-linear oscillations and stability of a column with a follower force.

12. P. J. HOLMES 1977 *Journal of Sound and Vibration* **53**, 471–503. Bifurcations to divergence and flutter in flow-induced oscillations: a finite dimensional analysis.
13. P. J. HOLMES and J. E. MARSDEN 1978 *Automatica* **14**, 367–384. Bifurcations to divergence and flutter in flow-induced oscillations: an infinite dimensional analysis.
14. J. E. MARSDEN and M. MCCRACKEN (Editors) 1976 *The Hopf Bifurcation and its Application.* New York: Springer Verlag.
15. D. SATTINGER 1973 *Topics in Stability and Bifurcation Theory, Springer Lecture Notes in Mathematics No.* 309. Berlin, Heidelberg, New York: Springer-Verlag.
16. P. J. HOLMES 1979 *Proceedings of the* 1978 *IEEE Conference on Decision and Control, Paper WA7*, 181–185. Global bifurcations and chaos in the forced oscillations of buckled structures.
17. D. R. J. CHILLINGWORTH 1976 *Differential Topology with a View to Applications.* London: Pitman.
18. V. K. MELNIKOV 1963 *Transactions of the Moscow Mathematical Society* **12**, 1–56. Stability of the center to time periodic perturbations.
19. P. J. HOLMES 1979 (to appear) *SIAM Journal on Applied Mathematics.* Averaging, global motions and chaos in forced oscillations.
20. S. SMALE 1967 *Bulletin of the American Mathematical Society* **73**, 747–817. Differentiable dynamical systems.
21. G. D. BIRKHOFF 1927 *Acta Mathematica* 359–367. On the periodic motions of dynamical systems.
22. C. S. HSU 1978 *Advances in Applied Mechanics* **17**, 245–301. On nonlinear parametric excitation problems.
23. Y. UEDA, C. HAYASHI and N. AKAMATSU 1973 *Electronics and Communications in Japan* **56**-A. 27–34. Computer simulation of nonlinear ordinary differential equations and nonperiodic oscillations.
24. Y. UEDA 1978 *Department of Electrical Engineering Preprint, Kyoto University.* Randomly transitional phenomena in the system governed by Duffing's equation.
25. J. CURRY 1978 *Communications in Mathematical Physics* **60**, 193–204. A generalized Lorenz system.
26. F. C. MOON 1977 in *Proceedings of the Conference on Noncontacting Suspension and Propulsion Systems for Advanced Ground Transportation,* Massachusetts Institute of Technology, (D. Wormley Editor). Printed by U.S. Department of Transportation. Static and dynamic instabilities in mag-lev model experiments.

APPENDIX A: COMMENTS ON THE REDUCTION OF DIMENSION— BIFURCATION THEORY AND INVARIANT MANIFOLDS

In deriving a theoretical model to explain the chaotic dynamics of the continuous beam (section 2), we have reduced a partial differential equation (21a, b), to a single degree of freedom model (22) by using Galerkin's method. As regards the static form of the system (21), classical bifurcation theory suffices as justification for the reduction to system (22) as is indicated below. For the full dynamical problem of section 3 more sophisticated techniques such as invariant manifold theory are necessary. Of course the two approaches are closely related.

As described in section 2.2, local static bifurcations or catastrophes occur as the magnet spacing is varied, and it may be possible to justify the discrete model of section 2.2 in terms of center manifold theory or, indeed, in terms of classical bifurcation theory [15]. Here we sketch how this might be done. The static bifurcation problem corresponding to equation (21) takes the form

$$Dv'''' - (Tv')' + (\partial\psi'/\partial\theta) - (\partial\psi/\partial v) \underline{\underline{\text{def}}}\, N(v, \mu) = 0 \tag{A1}$$

where the non-linear operator N contains parameters μ arising from the dependence of the magnetic field, and hence ψ, on factors such as magnet spacing. Clearly $v \equiv 0$ is a possible solution for all magnet positions, if one assumes perfect symmetry. Bifurcation from $v \equiv 0$ can occur when the operator $DN(0, \mu)$ is not invertible and the implicit function theorem fails. Here DN stands for the Fréchet derivative of N; in this case simply the linear part of N. If $DN(0, \mu)$ has a simple zero eigenvalue then bifurcation always occurs. In this case the

Liapunov–Schmidt procedure allows one to reduce the problem by projection methods to a one dimensional equation (see reference [15] for details).

In our case the eigenvalue problem can be approached via the Galerkin method. Expanding the displacement in an infinite set of orthonormal basis functions (22), one obtains, instead of the single equation (24), an infinite set of the form

$$m\ddot{a}_i + \Sigma a_j \left\{ \int_0^L [D\phi_j'' \phi_i'' - T\phi_j' \phi_i' + \kappa \phi_j' \phi_i'] \, ds \right\} = \int_0^L \mathscr{F}_y \phi_i \, ds - m\ddot{V}_0 \int_0^L \phi_i \, ds. \quad \text{(A2)}$$

Here the basis functions are assumed to satisfy the same boundary conditions as in section 3. If it is assumed that the magnetic field is concentrated at the tip as in section 2 and that the excitation is sinusoidal, one obtains an equation of the form

$$\ddot{a}_i + \Sigma \rho_{ij} a_j = (1/m) F_y \phi_i(L) + f_{0i} \cos \Omega t \quad \text{(A3)}$$

where, from equation (A2) $\rho_{ij} = \rho_{ji}$.

With F_y taken as an odd function of the tip displacement, F_y can be written as

$$F_y = m\alpha v(L) + (\text{cubic terms}) + \ldots = m\alpha \Sigma a_j \phi_j(L) + \text{h.o.t.}$$

When there is no excitation, the static bifurcations occur when one or more of the eigenvalues of this set of equations goes to zero. Thus if $a_i = A_i e^{i\omega_i t}$ then ω_i must satisfy

$$\Sigma[\rho_{ij} - \alpha \phi_j(L) \phi_i(L)] A_j = \omega_i^2 A_i. \quad \text{(A4)}$$

Note that the problem is self-adjoint and thus all eigenvalues are real. In the absence of magnets $\alpha = 0$, and $\omega_i^2 > 0$. As the magnets are brought in from a large distance, α increases monotonically (cf. Figure 5) until the smallest of these eigenvalues goes to zero, all others remaining bounded away from zero. Hence bifurcation occurs locally in the direction of the eigenfunction associated with $\omega_1 = 0$ [15]. This corresponds to part of the butterfly catastrophe. To capture the second bifurcations in which pairs of non-trivial equilibria are created one would have to vary a second parameter (corresponding to d in equation (9)) and to consider the cubic and quintic terms in detail. This is beyond the scope of the present, preliminary study.

The non-autonomous problem presents considerably greater difficulties, since the analysis of section 4 is global in nature and the bifurcation and center manifold theorems are local. However in reference [16] Holmes has approached a problem similar to equation (21) but in which the non-linear terms conveniently decouple in a Galerkin representation. This system has three equilibrium points, the trivial one being a saddle, and it is possible to show that, in the undamped, unforced system, the stable and unstable manifolds of the saddle point intersect to form a pair of homoclinic orbits just as in the single mode model analyzed later in section 4 (cf. reference [16], section 3). In the infinite dimensional problem these manifolds are each one dimensional and there is also a center manifold of codimension 2. On the addition of small forcing ($O(\varepsilon)$) and smaller damping ($O(\varepsilon^2)$) one can show that the stable manifold of the saddle becomes of codimension 1 and that it is therefore reasonable to expect the unstable manifold to intersect it and hence to expect that one has Smale horseshoes just as in the single mode problem. A complete study of this problem is now in progress. A key feature in this is the extension of the Melnikov method, outlined in section 4 and Appendix B, to infinite dimensional problems.

APPENDIX B: DETECTION OF HOMOCLINIC POINTS IN FORCED OSCILLATOR EQUATIONS

Given a system of the form

$$\dot{x} = y, \qquad \dot{y} = g(x) + \varepsilon(f \cos \omega t - \gamma y), \tag{B1}$$

which, for $\varepsilon = 0$, possesses a saddle-point $(0, 0)$ with a loop (or loops) Γ_0 connecting the seperatrices, we wish to investigate the structures near Γ_0 for $\varepsilon \neq 0$, small. Since, for $\varepsilon = 0$, system (B1) is Hamiltonian with Hamiltonian

$$H(x, y) = \frac{y^2}{2} + \int_0^x g(\zeta)\, d\zeta, \tag{B2}$$

the loop Γ_0 is given by the level curve $H(x, y) = 0$. Suppose one knows the solution of system (A1) for $\varepsilon = 0$ on Γ_0, and can write this solution $(x_0(t), y_0(t))$. Now when $0 < \varepsilon \ll 1$, there will be a saddle-type closed orbit γ_ε of period $2\pi/\omega$ near $(x, y) = (0, 0)$ [19]. Trajectories lying in the stable and unstable manifolds of γ_ε can be expressed in power series form as

$$\begin{aligned}(x^s(t), y^s(t)) &= (x_0(t) + \varepsilon x_1^s(t), y_0(t) + \varepsilon y_1^s(t)) + O(\varepsilon^2),\\ (x^u(t), y^u(t)) &= (x_0(t) + \varepsilon x_1^u(t), y_0(t) + \varepsilon y_1^u(t)) + O(\varepsilon^2),\end{aligned} \tag{B3}$$

the distance between the stable and unstable manifolds estimated as

$$\Delta(t_0) = \varepsilon[\dot{y}(t_0)(x_1^s(t_0) - x_1^u(t_0)) - \dot{x}(t_0)(y_1^s(t_0) - y_1^u(t_0))] + O(\varepsilon^2). \tag{B4}$$

$\Delta(t_0)$ is the (unnormalized) projection of the distance $\|(x_1^s, y_1^s) - (x_1^u, y_1^u)\|$ on to the normal $\hat{\mathbf{n}}(t_0)$ to the solution vector $(\dot{x}, \dot{y})$ at time t_0. Effectively one is here measuring the distance along $\hat{\mathbf{n}}$ between the manifolds, on a particular Poincaré section $\theta = \omega t_0 \in [0, 2\pi]$. Next one can allow t_0 to vary and, if $\Delta(t_0)$ has a simple zero at $t_0 = \tau$, it follows that the manifolds intersect transversely near $\hat{\mathbf{n}}(\tau)$ on the section $\theta = \tau$. See references [2, 18, 19] for more details.

In references [18] and [19] it is shown that, for a system of the form (B1), $\Delta(t_0)$ takes the form

$$\Delta(t_0) = \varepsilon \int_{-\infty}^{\infty} y_0(t - t_0)(f \cos \omega t - \gamma y_0(t - t_0))\, dt + O(\varepsilon^2). \tag{B5}$$

In calculating $\Delta(t_0)$ above, one finds (x_1^s, y_1^s) and (x_1^u, y_1^u) in equation (B4) essentially by solving the variational equation corresponding to equation (B1) linearized about $\Gamma_0 = (x_0, y_0)$. The analysis of references [18] and [19] is more general and the unperturbed system need not be Hamiltonian.

In the specific example of this paper one has (cf. reference [2]), taking $(A_1(0), A_2(0)) = (\sqrt{2}, 0)$,

$$(A_1, A_2) = (x_0(t), y_0(t)) = [\sqrt{2}\,\mathrm{sech}(t/\sqrt{2}), -\mathrm{sech}(t/\sqrt{2})\tanh(t/\sqrt{2})],$$

and thus

$$\Delta(t_0) = \varepsilon\left\{\int_{-\infty}^{\infty} -\gamma\,\mathrm{sech}^2\left(\frac{t - t_0}{\sqrt{2}}\right)\tanh^2\left(\frac{t - t_0}{\sqrt{2}}\right) dt - \int_{-\infty}^{\infty} f\,\mathrm{sech}\left(\frac{t - t_0}{\sqrt{2}}\right) \times \tanh\left(\frac{t - t_0}{\sqrt{2}}\right)\cos \omega t\, dt\right\} + O(\varepsilon^2).$$

The first integral is an exact differential and the second may be evaluated by the method of residues to obtain

$$\Delta(t_0) = -\varepsilon\{(2\sqrt{2}\gamma/3) + 2f\pi\omega[\sinh(\pi\omega/\sqrt{2})]^{-1} \sin \omega t_0\} + O(\varepsilon^2), \tag{B6}$$

from which one obtains equation (33). Note that, if $\gamma \ll f$, $\Delta(t_0)$ necessarily oscillates about zero and transversal intersections must occur.

In extending this procedure to a periodic perturbation of an infinite dimensional (partial differential) equation one must again assume that the unperturbed homoclinic orbit Γ_0 is known, say $(v, \dot{v}) = (v_0(x, t), \dot{v}_0(x, t))$. To compute approximate orbits in the perturbed manifolds one simply solves the variational equation corresponding to the perturbed system linearized about $(v_0, \dot{v}_0)$, as in the two dimensional case above. This leads to an expression for $\Delta(t_0)$ similar to expression (B5) but involving integrals (inner products) over the spatial extent of the beam. Again it appears that, if the modal damping coefficients are of order ε^2 and the force amplitude of order $\varepsilon(\varepsilon \ll 1)$, then $\Delta(t_0)$ must necessarily oscillate about zero. Details of the infinite dimensional case are to be published in a forthcoming paper.